ACS APPLIED MATERIALS & INTERFACES

Research Article

www.acsami.org

Confined Nanospace Synthesis of Less Aggregated and Porous Nitrogen-Doped Graphene As Metal-Free Electrocatalysts for Oxygen Reduction Reaction in Alkaline Solution

Xiangjie Bo, Ce Han, Yufan Zhang, and Liping Guo*

Faculty of Chemistry, Northeast Normal University, Changchun 130024, P. R. China

Supporting Information

ABSTRACT: A facile and low-emission strategy is used for preparation of porous nitrogen-doped graphene (NGR) in a confined nanospace. The negative charged graphene oxide (GO) serves as a substrate for deposition of electropositive metal amine complex and then thin layer of silica (SiO_2) is formed onto the copper amine ion-coated GO. Carbonization of copper amine ion-coated GO in a confined nanospace of SiO_2 and the subsequent removal of the Cu particles and SiO_2 layer produces less aggregated and porous nitrogen-doped graphene (NGR). NGR materials are highly active, cheap, and selective metal-free electrocatalysts for the oxygen reduction reaction (ORR) in alkaline solution. The electron transfer for ORR at NGR catalysts is found to be around 4 at potentials ranging from −0.35 to −0.70 V. NGR may be further exploited as potentially efficient and inexpensive nonmetal ORR catalysts with good selectivity and long-term stability in alkaline solution.

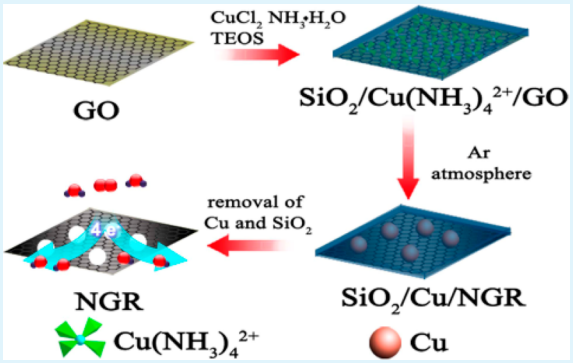

KEYWORDS: *nitrogen doping, graphene, oxygen reduction reaction, electrocatalysts, confined nanospace synthesis*

1. INTRODUCTION

Fuel cells have been recognized to be an environmentally friendly power source because of their cleanliness and high efficiency. The oxygen reduction reaction (ORR) at cathode is the key factor in determining the performance of a fuel cell. The ORR is effectively facilitated by Pt-based electrocatalysts, which show large cathodic current densities and low overpotentials. However, the wide application of Pt-based electrocatalysts is hindered by their high cost and sluggish kinetic toward ORR. The instability of Pt-based catalysts is derived from a loss in electrochemical surface area after prolonged usage. Then the loss of electrochemical surface area of Pt electrocatalysts contributes to a decrease in the ORR activity and thus a deterioration of performance in the overall fuel cells.[1] Replacement of Pt catalysts with metal-free catalysts would be desirable to facilitate the commercialization of fuel cells. One nonprecious metal alternative to Pt is nitrogen-doped carbon nanomaterials, which exhibits high ORR activity and good stability in alkaline solution. The nitrogen doping introduces structural defects and doped nitrogen with lone electron pairs provides negative charges. The carbon atoms adjacent to nitrogen with high positive charge density increase their interaction, which results in the enhanced ORR activity. Graphene (GR) doped with nitrogen,[2,3] boron,[4] sulfur,[5] phosphorus,[6] and halogen[7,8] have been applied as active catalysts for ORR with long-term stability and high methanol tolerance. GR sheets codoped with nitrogen and boron were successfully produced by simply annealing GO in the presence of boric acid under ammonia gas.[9] Due to a synergetic effect arising from nitrogen and boron codoping, the boron and nitrogen-doped GR showed a superb ORR performance without crossover effect and with a high catalytic activity in alkaline medium. Nitrogen and sulfur dual-doped porous GR catalysts exhibited better ORR performance than that of GR catalysts doped solely with sulfur atoms or with nitrogen atoms.[10] The common methods for preparation of NGR are: plasma process,[11,12] chemical vapor deposition (CVD),[13,14] direct chemical pyrolysis,[15−17] arc-discharge method,[18] treatment with ammonia gas[19] or thermal annealing approach.[2,20,21] NGR has shown improved conductivity and high catalytic activity for ORR with better long-term durability. However, NGR prepared from CVD suffers from the involvement of an expensive machine and the use of toxic organic compounds as carbon and nitrogen source (such as: acetonitrile or pyridine[14,22]). NGR can be prepared by thermal pyrolysis of graphene oxide (GO) in the presence of nitrogen-containing organic compound, such as pyrrole,[21] aniline,[20] dopamine,[23] or melamine.[2] Because of the volatility of organic vapor at elevated temperatures under a flowing atmosphere of inert gas, high nitrogen precursors/GO ratio is required to enhance the nitrogen content of NGR. At high temperature, the toxic nitrogen-containing gas produced by the decomposition of

Received: December 6, 2013
Accepted: January 23, 2014
Published: January 23, 2014

   dx.doi.org/10.1021/am405609d | ACS Appl. Mater. Interfaces 2014, 6, 3023−3030

organic compounds can be swept out by the flow gas and is harmful to environment and human health. Although most of nitrogen precursors are decomposed at high temperature, direct pyrolysis of melamine,[24] aniline,[25] dopamine,[26] and pyrrole[27] in the absence of GO at inert atmosphere can also produce carbon materials. Therefore, carbon residue derived from nitrogen precursors are more or less remains on the surface of GR during the pyrolysis of nitrogen precursors/GO mixture. It is reasonable to deduce the nitrogen atoms may not solely belong to GR. Hence, it is not confirmed that all nitrogen heteroatoms have been fully doped into the GR framework. The electrochemical activity may be partially originated from the carbon residue. So, it is desired to prepare nitrogen-doped GR without the introduction of any carbon residue to show the actual activity of NGR. Thermal annealing of GO in the presence of ammonia offers a facile method for simultaneous nitrogen doping and reduction of GO without the introduction of any carbon residue.[19] However, high emission of toxic ammonia is accompanied by the reduction of GO under a flow of ammonia gas. During this process the GR sheets tend to form irreversible agglomerates or even restack to form graphite through $\pi-\pi$ stacking.[28,29] The irreversible agglomeration leads to the partial overlapping of the GR sheets and lowers the surface area of GR. The stacking also blocks the diffusion path of GR and sets a high resistance for the diffusion of reactant molecules.

Herein, silica-protected (SiO_2) pyrolysis process for preparing porous NGR with high surface area is presented. The preparation of NGR is presented in Scheme 1. The negative

Scheme 1. Preparation Pathway of NGR

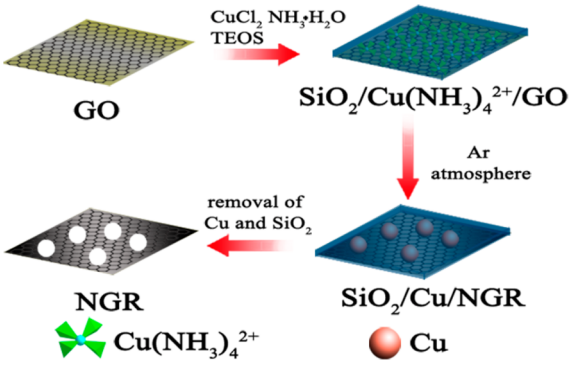

charged GO is used as a substrate for the growth of copper amine complex. Electropositive copper amine ions are first adsorbed onto both sides of GO and uniform layers of SiO_2 are simultaneously formed on GO. Confined nanospace pyrolysis and selective etching give rise to highly dispersed and porous NGR. The copper amine complex sandwiched between the GO and SiO_2 shells serves two functions: (1) ammonia ligands are used as nitrogen precursors for functionalization of GR by doping without the introduction of any carbon residue; (2) the redox reaction between copper ions and carbon atoms of GR facilitates the doping of nitrogen and formation of pores at NGR surface. The SiO_2 shells can not only prevent the escape of volatile nitrogen species from the surface of GO at high temperature but also prevent the irreversible stacking of NGR during the heteroatom doping process. Although dispersed NGR without pores was prepared by pyrolysis of GO under a flow of ammonia gas with the protection of mesoporous SiO_2,[30] the difference of our methodology is synthesis of porous NGR using an eco-friendly method with low emission of toxic gas. Compared with the nonporous GR, NGR catalysts exhibit superior electrochemical performance for ORR. As metal-free catalysts, NGR materials show much better fuel crossover resistance and long-term durability than the commercial Pt/C in alkaline medium.

2. EXPERIMENTAL SECTION

2.1. Materials. Nafion (5 wt %) was purchased from Sigma-Aldrich. Twenty wt % Pt/C commercial electrocatalysts were purchased from Johnson Matthey. Ammonia ($NH_3{\cdot}H_2O$), tetraethyl orthosilicate (TEOS), and copper chloride ($CuCl_2$) were purchased from Sinopharm Chemical Reagent Co., Ltd. China.

2.2. Apparatus and Electrochemical Test. X-ray diffraction (XRD) data were obtained on an X-ray D/max-2200vpc (Rigaku Corporation, Japan) instrument operated at 40 kV and 20 mA using Cu Kα radiation (k = 0.15406 nm). The SEM images were conducted on Philips XL-30 ESEM. TEM images were obtained at JEM-2100F transmission electron microscope (JEOL, Japan) operating at 200 kV. The nitrogen adsorption−desorption isotherms were performed on a Micromeritics ASAP 2020 instrument. The Brunauer−Emmett−Teller (BET) method was used for calculation of the specific surface area. The pore size distribution was derived from the adsorption branch by using the Barrett−Joyner−Halenda model. Electrochemical experiments were obtained at a Par 2273 Potentiostats-electrochemistry workstation. X-ray photoelectron spectroscopy (XPS) patterns were measured using Thermo ESCA LAB spectrometer (USA). A three-electrode configuration was employed, with a modified glassy carbon (GC, 3.0 mm in diameter (A = 0.07065 cm^2) for the examination for cyclic voltammogram (CV), 5.0 mm in diameter (A = 0.19625 cm^2) for the examination for rotating disk electrode (RDE).) electrode serving as the working electrode, and Ag/AgCl (in saturated KCl solution) and platinum wire serving as the reference and counter electrodes, respectively. CV experiments were conducted in 0.1 M KOH solution saturated with oxygen for ORR with the scan rate of 50 mV s^{-1}. Linear sweep voltammetric (LSV) tests on rotating disk electrode (RDE) were performed in 0.1 M KOH solution saturated with oxygen with rotation rates varying from 100 to 2500 rpm at 5 mV s^{-1}.

2.3. Preparation of NGR. GO was synthesized according to modified Hummers' method.[31,32] GO (0.32 g) was dispersed in 500 mL of distilled water and ethanol (V:V = 1:1). After ultrasonication for 6 h, 10 mL of $NH_3{\cdot}H_2O$ and 0.30 g of $CuCl_2$ were added into the mixture. Well-dispersed and negatively charged GO sheets can strongly interact with positively charged $Cu(NH_3)_4^{2+}$ ions to form a $Cu(NH_3)_4^{2+}$/GO composite. Five milliliters of TEOS was added dropwise into $Cu(NH_3)_4^{2+}$/GO composite solution under stirring. The above mixture was gently stirred for another 12 h at room temperature. Gray precipitates were collected by filtration and washed several times with double distilled water and then dried at 80 °C. Gray precipitates were pyrolyzed in a tube furnace under a flow of Ar at different temperature for 3 h. The composites were immersed into a 5% HF solution (40 mL) with stirring overnight. Then the black products were immersed into a 6 M HNO_3 solution (40 mL) with stirring overnight. NGR prepared at different pyrolysis temperature was denoted as NGR-X (X indicates the pyrolysis temperature.). For comparison, $Cu(NH_3)_4^{2+}$/GO nanosheets without protection of SiO_2 shells were directly treated under the same conditions and the composites obtained were named GR-1. Direct pyrolysis of SiO_2/GO without $Cu(NH_3)_4^{2+}$ produced dispersed GR without doping and the composites obtained were named GR-2. GR-1 and GR-2 were also treated with HF and HNO_3.

2.4. Fabrication of NGR or GR Modified Electrodes. The GC electrode was treated carefully with 1, 0.3, and 0.05 μm alumina powder, and then sonicated in water and absolute ethanol between each polishing step. Two milligrams of GR or NGR-X was dispersed in 1 mL of solvent mixture of Nafion (0.5 wt %) by sonication. The commercially available catalysts of Pt/C (Johnson Matthey) were used and 2 mg mL^{-1} of Pt/C suspension is also prepared as the same

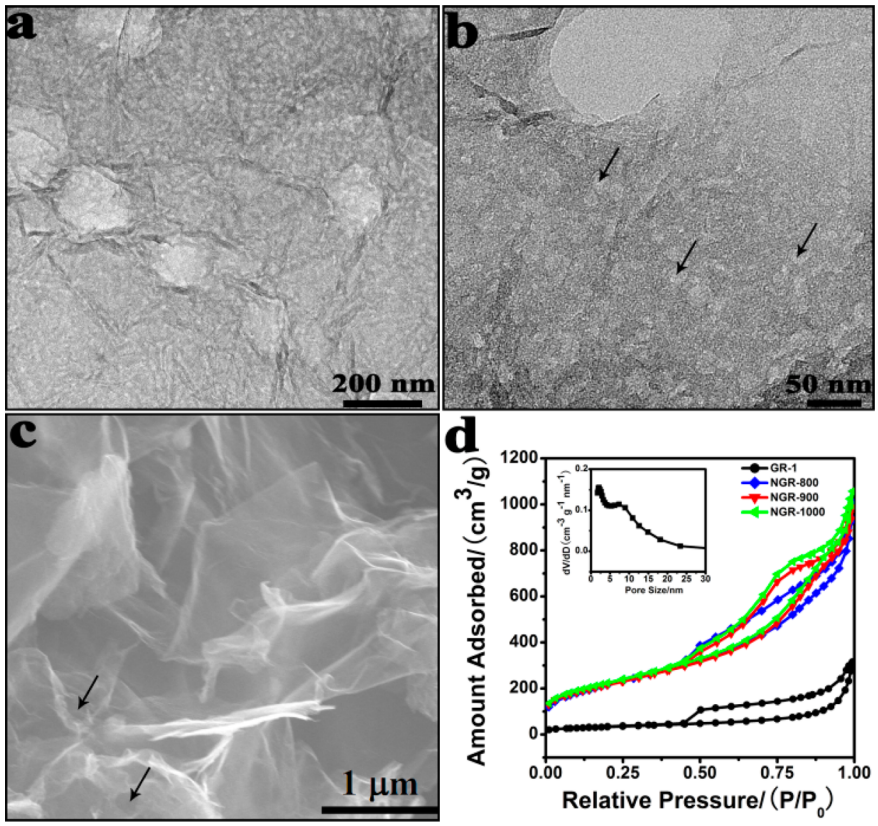

Figure 1. (a, b) TEM images of NGR-900. (c) SEM image of NGR-900. (d) Nitrogen adsorption−desorption isotherms of NGR-800, NGR-900, NGR-1000, and GR-1. Inset: Pore size distribution of NGR-900.

procedure as NGR-*X*. The electrode was dried at room temperature after 5 μL of the different catalyst was dropped onto the GC (3.0 mm) electrode surface. For RDE measurements, 14 μL of the suspension was dropped onto the GC (5.0 mm) electrode surface. In our work, loading amount of different catalysts was 0.14 mg cm^{-2} (geometric surface area of GC).

3. RESULTS AND DISCUSSION

The procedure for preparation of NGR was monitored by XRD. Figure S1 in the Supporting Information presents the XRD patterns of different composites. After the introduction of oxygen-containing functional groups on the GO surface, the XRD curve of GO shows a sharp peak at 10.26°, corresponding to a layered structure with a basal spacing of 0.86 nm. This value is higher than that of original graphite (0.34 nm). After thermal pyrolysis of $SiO_2/Cu(NH_3)_4^{2+}$/GO under Ar at 900 °C, the disappearance of the peak at 10.26° and the presence of Cu peaks indicates the efficient reduction of GO and formation of Cu species. At high temperature, the Cu ions are reduced to Cu species by carbon atoms. The NGR-900 exhibits an interlayer spacing of 0.35 nm, which is close to the *d*-spacing of natural graphite. This difference between SiO_2/Cu/NGR-900 and NGR-900 strongly suggests that Cu residues have been largely removed by acid etching.

Figure S2a in the Supporting Information presents the SEM image of GO. SEM image of GO displays a curled morphology consisting of a thin wrinkled paperlike structure. The SEM image of $SiO_2/Cu(NH_3)_4^{2+}$/GO reflects that SiO_2 shell is homogeneously coated on the both sides of GO (see Figure S2b in the Supporting Information). Removal of SiO_2 shell and Cu particles results in a highly dispersed NGR-900 with some pores that were originally occupied by Cu species. The SEM image of GR-2 exhibits the layer structure without pores (see Figure S2c in the Supporting Information). Comparison between GR-1 and GR-2 indicates GR-2 have a dispersed structure, reflecting that SiO_2 shell can effectively prevent the aggregation of GR-2. GR-1 prepared without protection of SiO_2 exhibits an aggregated morphology.

TEM analyses were conducted to determine the microstructure of SiO_2/Cu/NGR and NGR-900. From the TEM image of SiO_2/Cu/NGR in Figure S3a in the Supporting Information, some Cu particles with different diameter can be clearly observed on GR sheet. TEM observation of GR-2 indicates GR-2 is transparent with the voile-like structure (see Figure S3b in the Supporting Information). TEM image of NGR-900 (Figure 1a) shows that the voile-like structure is basically remained after introduction of nitrogen into GR. However, many large pores with the size of 100−150 nm generated by removal of Cu particles are clearly observed on the sheets. In Figure 1b some mesopores around 10 nm are randomly visible on the surface of NGR-900 (marked by arrow). The carbon atoms of NGR-900 serve as a sacrificial reductant to reduce Cu ions and the subsequent removal of the Cu nanoparticles generates NGR-900 with a porous structure. From the SEM image of NGR-900 (Figure 1c), some large pores are founded on the surface of NGR-900, which is consistent with the TEM image (Please note at this scale of SEM image, the mesopores around 10 nm are difficult to be seen.). This observation, obtained from SEM and TEM, indicates porous and dispersed NGR-900 can be successfully fabricated by confined strategy in Scheme 1. The porous nature of three NGR at different pyrolysis temperature and GR-1 without silica protection was further characterized by nitrogen

adsorption isotherm, which allows the calculation of specific surface area and pore size distribution. Figure 1d presents the nitrogen adsorption−desorption isotherms of NGR-800, NGR-900, and NGR-1000. The BET specific surface areas of NGR-800, NGR-900, and NGR-1000 are 643, 771, and 801 $m^2\ g^{-1}$, respectively. The nitrogen adsorption−desorption isotherm of NGR-900 exhibits a BET value of 771 $m^2\ g^{-1}$. NGR-900 exhibits a binary pore distribution at 2.1 and 7.5 nm (inset of Figure 1d). The high surface area of NGR-900 facilitates the exposure of active sites for catalysis. The porous structure is favorable for the mass transfer of molecules. The BET surface area of NGR-900 is higher than GR-1 (118 $m^2\ g^{-1}$) and those reported for GR and NGR.[33−37] The SiO_2 on the surface of GO is beneficial for decreasing the aggregation of NGR sheets and highly dispersed porous NGR is obtained.

The formation of NGR was characterized by XPS. From the XPS spectra in Figure S4a in the Supporting Information, the peaks associated with C−O and C═O are predominant for GO. After thermal reduction of GO, the corresponding XPS spectrum (see Figure S4b in the Supporting Information) shows a strong suppression for the oxygen-containing components of C1s. The result indicates the efficient removal of the oxygen-containing groups in GO by thermal reduction. Figure 2 shows XPS patterns of NGR at different pyrolysis

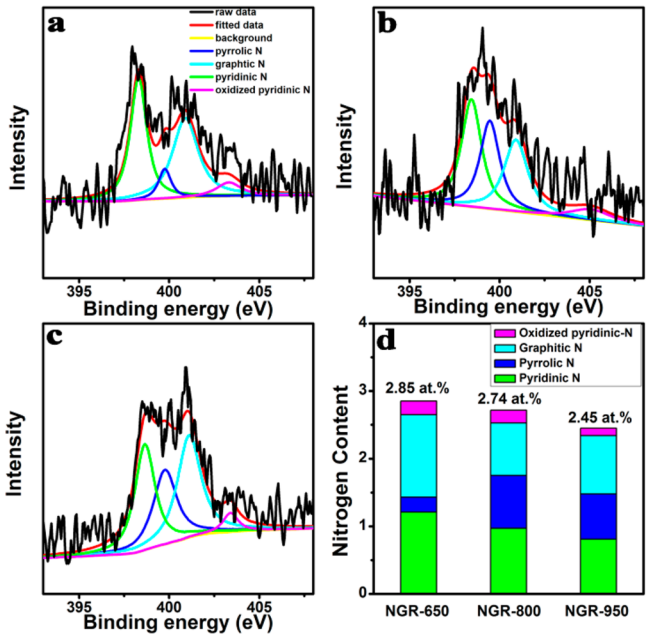

Figure 2. N 1s XPS spectra of (a) NGR-800, (b) NGR-900, and (c) NGR-1000. (d) The content of N-bonding configurations in three NGR sample at different pyrolysis temperature.

temperature. When the pyrolysis temperature is increased from 800 to 1000 °C, the total nitrogen content are 2.85, 2.74, and 2.45 at % for NGR-800, NGR-900, and NGR-1000, respectively. Unlike the obvious decreased nitrogen content at high temperature,[3] nitrogen loss in NGR during pyrolysis at high temperatures is alleviated by the protection of SiO_2 shell. However, no peak related to N 1s is observed at $Cu(NH_3)_4^{2+}$/GO without protection of SiO_2 shell (see Figure S4c in the Supporting Information), indicating SiO_2 shell can effectively trap the volatile nitrogen species sandwiched between SiO_2 shell and GO and facilitates the doping of nitrogen. The redox reaction between the Cu ions and carbon atoms causes the C−C bond cleavage and defects in NGR. The defects provide active sites for nitrogen doping into GR framework. In addition, no trace of Cu element is visible from XPS spectrum (see Figure S4d in the Supporting Information). The absence of Cu 2p in XPS clearly indicates the complete removal of Cu species from the NGR-900, which is well-consistent with the XRD result.

The catalytic activity of NGR-900 toward ORR was tested by CVs in a three-electrode cell in oxygen-saturated 0.1 M KOH. Figure 3a shows the electrochemical reduction of oxygen at GR-1 (black line), GR-2 (red line), NGR-900 (green line), and Pt/C catalysts (blue line). Commercial Pt/C catalysts exhibit a reduction peak at −0.16 V for ORR. As can be seen, a cathodic peak for ORR around −0.30 V is observed at GR-1 and GR-2 catalysts. Compared with GR-1 and GR-2, a significant increase of peak current density and an obvious positive shift of peak potential can be found on NGR-900 (green line). NGR-900 catalysts exhibit a substantial reduction process in the presence of oxygen with the cathodic reduction peak at around −0.25 V. The peak potential for reduction of oxygen at NGR-900 is more positive than that of GR-1 and GR-2, shifting positively by about 50 mV. The higher peak current density and more positive reduction potential observed from CVs suggests NGR-900 catalysts exhibit much better catalytic activity toward ORR than GR-1 and GR-2. LSVs on RDE in Figure 3b were conducted to further investigate the ORR activity of NGR-900 and compare it with commercial Pt/C catalysts. In agreement with the voltammetric data, GR-1 and GR-2 catalysts without doping exhibit poor activity for ORR. As shown in Figure 3b, the onset potential of ORR at GR-1 and GR-2 electrode commences around −0.22 V, whereas the onset potential at NGR-900 catalysts significantly shifts positively to −0.13 V with the limiting diffusion current density at −0.70 V being about 1.5 times larger than that of GR-2. The obvious enhancement in current density for NGR-900 indicates the high ORR activity of NGR-900. The onset potential of the ORR on NGR-900 is more positive than that of GR-1 and GR-2, but still negatively shifts from the value for Pt/C catalysts (−0.06 V).

To select the optimum pyrolysis temperature for subsequent work, it is important to study the catalytic activity of NGR with different pyrolysis temperature. The electrochemical data in Figure 4a compare the effect of pyrolysis temperature on ORR activity in 0.1 M KOH. Compared with NGR-800 and NGR-1000, a remarkable enhancement of catalytic activity is observed at NGR-900. The cathodic current is about −1.29 mA cm^{-2} at NGR-900, compared to −0.88 mA cm^{-2} at NGR-800 and −0.95 mA cm^{-2} at NGR-1000. This observation reflects the superior performance of NGR-900 over NGR-800 and NGR-1000 as catalysts for ORR. Although the active site in nitrogen-doped carbon materials for ORR is still controversial,[38−41] insights from the published literatures confirm that pyridinic N and pyrrolic N are the predominant origin of electrochemical activity for ORR.[38,42] The content of graphitic N is in the order NGR-800 > NGR-1000 > NGR-900. From the electrochemical data, NGR catalysts with low content of graphitic N show high activity for ORR. Considering the N bonding configurations in NGR at different pyrolysis temperature (Figure 2d), the enhancement in the cathodic response of NGR-900 is ascribed to high content of pyridinic N and pyrrolic N of NGR-900. In addition, the high surface area of NGR catalysts is favorable for the exposure of active sites for ORR. The low activity of NGR-800 is due to the low content of

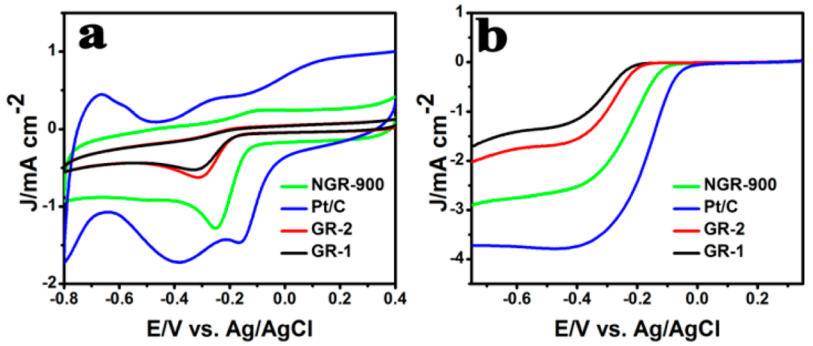

Figure 3. (a) CVs and (b) LSV curves of NGR-900 (green line), GR-1 (black line), GR-2 (red line), and Pt/C (blue line) in oxygen-saturated 0.1 M KOH. Scan rate of CVs, 50 mV s^{-1}; scan rate of LSVs, 5 mV s^{-1}; rotation rate, 1200 rpm.

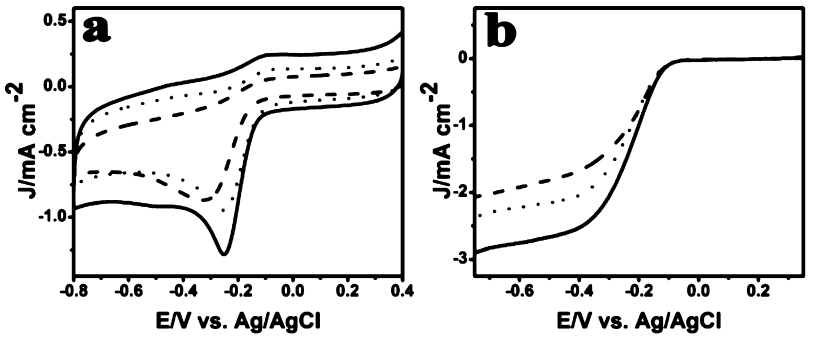

Figure 4. (a) CVs of NGR-800 (dash line), NGR-900 (solid line), and NGR-1000 (dot line) in oxygen-saturated 0.1 M KOH. Scan rate, 50 mV s^{-1}. (b) LSV curves of NGR-800 (dash line), NGR-900 (solid line), and NGR-1000 (dot line) in oxygen-saturated 0.1 M KOH. Scan rate, 5 mV s^{-1}; rotation rate, 1200 rpm.

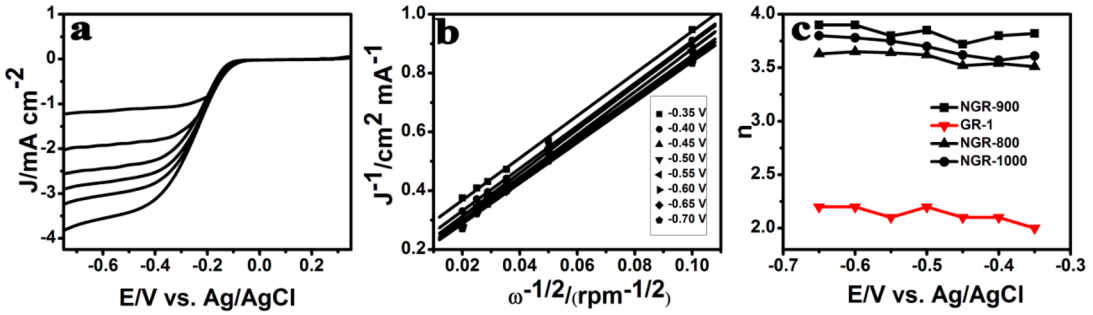

Figure 5. (a) LSV curves at different rotation rates recorded for ORR at NGR-900 in oxygen-saturated 0.1 M KOH. Scan rate: 5 mV s^{-1}. Rotation rate: 100, 400, 800, 1200, 1600, and 2500 rpm. (b) Koutecky–Levich plots of NGR-900 at different electrode potentials. (c) The dependence of electron transfer number *n* on potential for NGR-800, NGR-900, NGR-1000, and GR-1.

pyridinic N and pyrrolic N and its low surface area. NGR-900 and NGR-1000 exhibit almost the same specific area (Figure 1d). However, NGR-900 has a high content of pyridinic N and pyrrolic N. NGR-900 exhibits a high activity for ORR. Figure 4b shows the LSVs of NGR at different pyrolysis temperature. In agreement with the voltammetric data, the plateau current of NGR-900 is higher than these of NGR-800 and NGR-1000. The high plateau current density obtained at NGR-900 indicates that NGR-900 have better electrocatalytic activity for ORR. On the basis of the above optimization, NGR-900 is selected for subsequent work. In addition, the optimization of $Cu(NH_3)_4^{2+}$/GO ratio and characterization of the obtained NGR has been conducted. NGR prepared at 900 °C with 0.15 and 0.60 g of $CuCl_2$ was denoted as NGR-900−0.15 and NGR-900−0.60, respectively. When 0.15 g of $CuCl_2$ was used, due to the low concentration of copper ions, the nitrogen content in the NGR-900−0.15 is low (1.32%, see Figure S5c in the Supporting Information). The TEM image of NGR-900−0.15 exhibits porous structure (see Figure S5a in the Supporting Information). The low ORR activity in Figure S5e in the Supporting Information of NGR-900−0.15 (red line) is presumably because of its low nitrogen content (see Figure S5c in the Supporting Information) and its low surface area (372 m^2 g^{-1}, see inset of Figure S5a in the Supporting Information). However, with a high amount of $CuCl_2$ (0.60 g), large pores isare observed from the TEM image (see Figure S5b in the Supporting Information) and a high content of nitrogen is introduced into NGR-900−0.60 (3.31%, see Figure S5d in the Supporting Information). More nitrogen atoms are introduced into the framework of NGR-900−0.60 with a large amount of $CuCl_2$. Compared with the NGR-900 with use of 0.30 g of $CuCl_2$, only a little high ORR activity is obtained at NGR-900−0.60 (blue line), even the content of pyridinic N and pyrrolic N for NGR-900−0.60 is higher than NGR-900.

dx.doi.org/10.1021/am405609d | ACS Appl. Mater. Interfaces 2014, 6, 3023−3030

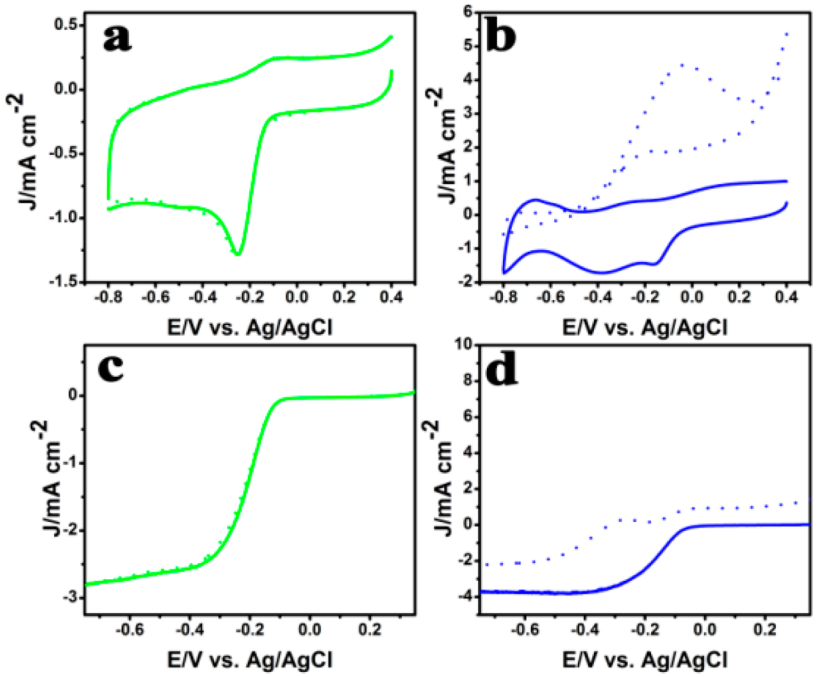

Figure 6. (a) CVs and (c) LSV curves of NGR-900 in oxygen-saturated 0.1 M KOH (green solid line) and oxygen-saturated 0.1 M KOH containing 3 M methanol (green dot line). (b) CVs and (d) LSV curves of Pt/C in oxygen-saturated 0.1 M KOH (blue solid line) and oxygen-saturated 0.1 M KOH containing 3 M methanol (blue dot line).

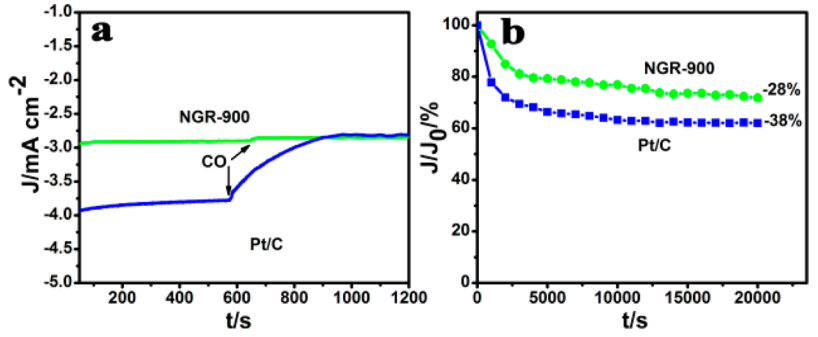

Figure 7. (a) CO-poison effect on the current−time response for the NGR-900 (green line) and Pt/C (blue line) at −0.35 V. The arrow indicates the addition of 10% (volume/volume) CO gas into oxygen-saturated 0.1 M KOH. (b) The relative decrease in the current density with time for NGR-900 (green line) and Pt/C (blue line).

This small discrepancy in the ORR activity between NGR-900 and NGR-900−0.60 is ascribed to their different porosity. As we know, with more copper, more carbon atoms are consumed to reduce the copper ions. More depleted carbon leads to large pores and then decrease of BET surface area is observed (inset of Figure S5b in the Supporting Information). The low surface area (493 m^2 g^{-1}) of NGR-900−0.60 is not favorable for providing surface catalytic sites exposed to oxygen molecules and thus results in ORR activity decrease. The high content of nitrogen of NGR-900−0.60 is counteracted by its low surface area. In addition, due to redox reaction between the carbon atoms and more copper ions, the low productivity of NGR-900−0.60 with more copper ions makes it unsuitable for large-scale use in ORR. Taking into account the productivity and ORR activity, NGR-900 with the use of 0.30 g of $CuCl_2$ is used in subsequent experiments.

Figure 5a shows the LSVs of NGR-900 in oxygen-saturated 0.1 M KOH electrolyte over a range of electrode rotation rates. As can be seen, an increase in the catalytic current with rotation rate is observed for NGR-900. The Koutecky−Levich plots (J^{-1} vs $\omega^{-1/2}$) at different electrode potentials display good linearity (Figure 5b). The number (n) of electron transferred during ORR is calculated on the basis of the Koutecky−Levich equation

$$\frac{1}{J} = \frac{1}{J_k} + \frac{1}{B\omega^{0.5}}$$

where J_k is the kinetic current density and B is related to the diffusional current density. B is related to the diffusion-limiting current density expressed by the following expression

$$B = 0.2nFD^{2/3}\nu^{-1/6}C_{O_2}$$

where n is the number of electrons exchanged per oxygen molecule, F is the Faraday constant (96485 C mol^{-1}), ν is the kinematic viscosity of the electrolyte (1.13×10^{-2} cm^2 s^{-1}), D is the oxygen diffusion coefficient (1.9×10^{-5} cm^2 s^{-1}), and C_{O_2} is the bulk concentration of oxygen (1.2×10^{-3} mol L^{-1}). The dependence of n on the potential at NGR-900 electrode is shown in Figure 5c. The value of n for NGR-900 at −0.35 V is

dx.doi.org/10.1021/am405609d | ACS Appl. Mater. Interfaces 2014, 6, 3023−3030

found to be 3.8 and increases to 3.9 at more negative potentials, indicating that oxygen reduction follows mainly the 4 electron pathway. In agreement with the electrochemical data, the *n* of NGR-900 is higher than that of NGR-800 and NGR-1000. In contrast, the number of electron transferred per O_2 for GR-1 is calculated to be around 2.0. These results suggest that NGR-900 with high content of pyridinic N and pyrrolic N show much better electrocatalytic activity toward ORR than the pristine GR-1. Our result is consistent with the published literatures.[38,42]

To examine the selectivity for ORR on NGR-900 and Pt/C catalysts, we performed methanol crossover test in the current−time measurement. Figure 6a shows the CVs of NGR-900 in oxygen-saturated 0.1 M KOH with or without 3 M methanol. No noticeable decrease of response was observed for NGR-900. This result reflects that NGR-900 catalysts possess a high selectivity for the ORR. However, Pt/C catalysts exhibit a substantially larger current for the oxidation of methanol reflecting the low tolerance to fuel crossover effect (Figure 6b). The higher methanol tolerance of NGR-900 during ORR compared with Pt/C indicates that NGR-900 may function as a methanol-tolerant cathode in fuel cells. Comparison between panels c and d in Figure 6 also indicates the better tolerance of methanol at NGR-900 than that of Pt/C. The CO poisoning effect can result in instability as well as a reduction in cathodic performance at Pt-based ORR catalysts. CO poisoning was tested to show the high selectivity and good tolerance of NGR-900. The effect of CO on the electrocatalytic activity of the NGR-900 is also tested in Figure 7a. When 10% CO (volume/volume) is introduced into the testing cell, only 4% current diminutions are observed for NGR-900 catalysts, showing high catalytic selectivity for ORR against CO poisoning (green line). In contrast, the obvious oxidation of CO on commercial Pt/C seriously inhibits the ORR process, as indicated by the disappearance of ORR current. In contrast, the NGR-900 is nonplatinum catalysts for ORR. NGR-900 catalysts exhibit excellent catalytic activity for ORR in alkaline medium with high tolerance to CO and methanol. This result indicates that the NGR-900 is a good alternative to Pt as cathode catalysts.

The durability of the catalysts and the long-term stability of the electrocatalytic activity for ORR are of prominent concern in fuel cells. Another attractive feature of the NGR-900 catalysts is their highly stable amperometric response toward ORR. Pt/C catalysts display a rapid decay of the signal (up to 38%) current depression after 20000 s, indicating a poor stability (blue line in Figure 7b). In contrast, the response of NGR-900 electrode retains acceptable stability throughout the entire experiment, with only 28% current diminutions at 20000 s (green line in Figure 7b). This result demonstrates the higher durability of NGR-900 compared with Pt/C.

CONCLUSIONS

Highly dispersed and porous NGR with large surface area is prepared using a confined method with low emission of toxic gas. With the protection of SiO_2 shell, ammonia ligands from $Cu(NH_3)_4^{2+}$ can be doped into the framework of GR without introduction of any other carbon residue. Less aggregated and porous NGR materials are highly active, cheap, and selective metal-free electrocatalysts for ORR in alkaline solution. NGR catalysts exhibit excellent catalytic activity for ORR in alkaline medium with higher selectivity and better long-term stability than commercial Pt/C catalysts. NGR can be further developed as potentially efficient and inexpensive metal-free ORR catalysts with good long-term stability in alkaline solution.

ASSOCIATED CONTENT

Supporting Information

XRD patterns of GO, SiO_2/Cu/NGR, and NGR-900. SEM images of GO, $SiO_2/Cu(NH_3)_4^{2+}$/GO, GR-2, and GR-1. TEM images of SiO_2/Cu/NGR-900 and GR-2. C 1s XPS spectra of GO and NGR-900. N1s spectrum of GR-1. Cu 2p XPS spectrum of NGR-900. The optimization of $Cu(NH_3)_4^{2+}$/GO ratio. This material is available free of charge via the Internet at http://pubs.acs.org.

AUTHOR INFORMATION

Corresponding Author

*E-mail: guolp078@nenu.edu.cn.

Notes

The authors declare no competing financial interest.

ACKNOWLEDGMENTS

The authors gratefully acknowledge the financial support of the National Natural Science Foundation of China (21075014) and the Fundamental Research Funds for the Central Universities (10SSXT141).

REFERENCES

(1) Ferreira, P. J.; la O, G. J.; Shao-Horn, Y.; Morgan, D.; Makharia, R.; Kocha, S.; Gasteiger, H. A. Instability of Pt/C Electrocatalysts in Proton Exchange Membrane Fuel Cells−A Mechanistic Investigation. *J. Electrochem. Soc.* **2005**, *152*, A2256−A2271.

(2) Sheng, Z.-H.; Shao, L.; Chen, J.-J.; Bao, W.-J.; Wang, F.-B.; Xia, X.-H. Catalyst-Free Synthesis of Nitrogen-Doped Graphene via Thermal Annealing Graphite Oxide with Melamine and Its Excellent Electrocatalysis. *ACS Nano* **2011**, *5*, 4350−4358.

(3) Yang, S.; Feng, X.; Wang, X.; Müllen, K. Graphene-Based Carbon Nitride Nanosheets as Efficient Metal-Free Electrocatalysts for Oxygen Reduction Reactions. *Angew. Chem., Int. Ed.* **2011**, *50*, 5339−5343.

(4) Sheng, Z.-H.; Gao, H.-L.; Bao, W.-J.; Wang, F.-B.; Xia, X.-H. Synthesis of Boron Doped Graphene for Oxygen Reduction Reaction in Fuel Cells. *J. Mater. Chem.* **2012**, *22*, 390−395.

(5) Yang, Z.; Yao, Z.; Li, G.; Fang, G.; Nie, H.; Liu, Z.; Zhou, X.; Chen, X.; Huang, S. Sulfur-Doped Graphene As an Efficient Metal-Free Cathode Catalyst for Oxygen Reduction. *ACS Nano* **2012**, *6*, 205−211.

(6) Zhang, C.; Mahmood, N.; Yin, H.; Liu, F.; Hou, Y. Synthesis of Phosphorus-Doped Graphene and Its Multifunctional Applications for Oxygen Reduction Reaction and Lithium Ion Batteries. *Adv. Mater.* **2013**, *25*, 4932−4937.

(7) Yao, Z.; Nie, H.; Yang, Z.; Zhou, X.; Liu, Z.; Huang, S. Catalyst-Free Synthesis of Iodine-Doped Graphene via a Facile Thermal Annealing Process and Its Use for Electrocatalytic Oxygen Reduction in an Alkaline Medium. *Chem. Commun.* **2012**, *48*, 1027−1029.

(8) Jeon, I.-Y.; Choi, H.-J.; Choi, M.; Seo, J.-M.; Jung, S.-M.; Kim, M.-J.; Zhang, S.; Zhang, L.; Xia, Z.; Dai, L. Facile, Scalable Synthesis of Edge-Halogenated Graphene Nanoplatelets As Efficient Metal-Free Eletrocatalysts for Oxygen Reduction Reaction. *Sci. Rep.* **2013**, *3*, 1810.

(9) Wang, S.; Zhang, L.; Xia, Z.; Roy, A.; Chang, D. W.; Baek, J.-B.; Dai, L. BCN Graphene as Efficient Metal-Free Electrocatalyst for the Oxygen Reduction Reaction. *Angew. Chem., Int. Ed.* **2012**, *51*, 4209−4212.

(10) Liang, J.; Jiao, Y.; Jaroniec, M.; Qiao, S. Z. Sulfur and Nitrogen Dual-Doped Mesoporous Graphene Electrocatalyst for Oxygen Reduction with Synergistically Enhanced Performance. *Angew. Chem., Int. Ed.* **2012**, *51*, 11496−11500.

(11) Wang, Y.; Shao, Y.; Matson, D. W.; Li, J.; Lin, Y. Nitrogen-Doped Graphene and Its Application in Electrochemical Biosensing. *ACS Nano* **2010**, *4*, 1790−1798.
(12) Kumar, N. A.; Nolan, H.; McEvoy, N.; Rezvani, E.; Doyle, R. L.; Lyons, M. E. G.; Duesberg, G. S. Plasma-Assisted Simultaneous Reduction and Nitrogen Doping of Graphene Oxide Nanosheets. *J. Mater. Chem. A* **2013**, *1*, 4431−4435.
(13) Reddy, A. L. M.; Srivastava, A.; Gowda, S. R.; Gullapalli, H.; Dubey, M.; Ajayan, P. M. Synthesis Of Nitrogen-Doped Graphene Films For Lithium Battery Application. *ACS Nano* **2010**, *4*, 6337−6342.
(14) Imamura, G.; Saiki, K. Synthesis of Nitrogen-Doped Graphene on Pt(111) by Chemical Vapor Deposition. *J. Phys. Chem. C* **2011**, *115*, 10000−10005.
(15) Li, X. H.; Kurasch, S.; Kaiser, U.; Antonietti, M. Synthesis of Monolayer-Patched Graphene from Glucose. *Angew. Chem., Int. Ed.* **2012**, *51*, 9689−9692.
(16) He, C.; Li, Z.; Cai, M.; Cai, M.; Wang, J.-Q.; Tian, Z.; Zhang, X.; Shen, P. K. A Strategy for Mass Production of Self-Assembled Nitrogen-Doped Graphene As Catalytic Materials. *J. Mater. Chem. A* **2013**, *1*, 1401−1406.
(17) Pan, F.; Jin, J.; Fu, X.; Liu, Q.; Zhang, J. Advanced Oxygen Reduction Electrocatalyst Based on Nitrogen-Doped Graphene Derived from Edible Sugar and Urea. *ACS Appl. Mater. Interfaces* **2013**, *5*, 11108−11114.
(18) Panchakarla, L. S.; Subrahmanyam, K. S.; Saha, S. K.; Govindaraj, A.; Krishnamurthy, H. R.; Waghmare, U. V.; Rao, C. N. R. Synthesis, Structure, and Properties of Boron- and Nitrogen-Doped Graphene. *Adv. Mater.* **2009**, *21*, 4726−4730.
(19) Li, X.; Wang, H.; Robinson, J. T.; Sanchez, H.; Diankov, G.; Dai, H. Simultaneous nitrogen doping and reduction of graphene oxide. *J. Am. Chem. Soc.* **2009**, *131*, 15939−15944.
(20) Lin, Z.; Waller, G. H.; Liu, Y.; Liu, M.; Wong, C.-p. Simple Preparation of Nanoporous Few-Layer Nitrogen-Doped Graphene for Use As an Efficient Electrocatalyst for Oxygen Reduction and Oxygen Evolution Reactions. *Carbon* **2013**, *53*, 130−136.
(21) Jiang, S.; Zhu, C.; Dong, S. Cobalt and Nitrogen-Cofunctionalized Graphene As a Durable NonPrecious Metal Catalyst with Enhanced ORR Activity. *J. Mater. Chem. A* **2013**, *1*, 3593−3599.
(22) Jin, Z.; Yao, J.; Kittrell, C.; Tour, J. M. Large-Scale Growth and Characterizations of Nitrogen-Doped Monolayer Graphene Sheets. *ACS Nano* **2011**, *5*, 4112−4117.
(23) Cong, H.-P.; Wang, P.; Gong, M.; Yu, S.-H. Facile Synthesis of Mesoporous Nitrogen-Doped Graphene: An Efficient Methanol−tolerant Cathodic Catalyst for Oxygen Reduction Reaction. *Nano Energy* **2014**, *3*, 55−63.
(24) Li, X.; Zhang, J.; Shen, L.; Ma, Y.; Lei, W.; Cui, Q.; Zou, G. Preparation and Characterization of Graphitic Carbon Nitride through Pyrolysis of Melamine. *Appl. Phys. A: Mater. Sci. Process.* **2009**, *94*, 387−392.
(25) Silva, R.; Voiry, D. A.; Chhowalla, M.; Asefa, T. Efficient Metal-Free Electrocatalysts for Oxygen Reduction: Polyaniline-Derived N- and O-Doped Mesoporous Carbons. *J. Am. Chem. Soc.* **2013**, *135*, 7823−7826.
(26) Ai, K.; Liu, Y.; Ruan, C.; Lu, L.; Lu, G. M. Sp^2 C-Dominant N-Doped Carbon Sub-micrometer Spheres with a Tunable Size: A Versatile Platform for Highly Efficient Oxygen-Reduction Catalysts. *Adv. Mater.* **2012**, *25*, 998−1003.
(27) Morozan, A.; Jégou, P.; Campidelli, S.; Palacin, S.; Jousselme, B. Relationship between Polypyrrole Morphology and Electrochemical Activity Towards Oxygen Reduction Reaction. *Chem. Commun.* **2012**, *48*, 4627−4629.
(28) Si, Y.; Samulski, E. T. Exfoliated Graphene Separated by Platinum Nanoparticles. *Chem. Mater.* **2008**, *20*, 6792−6797.
(29) Stankovich, S.; Dikin, D. A.; Piner, R. D.; Kohlhaas, K. A.; Kleinhammes, A.; Jia, Y.; Wu, Y.; Nguyen, S. T.; Ruoff, R. S. Synthesis of Graphene-Based Nanosheets via Chemical Reduction of Exfoliated Graphite Oxide. *Carbon* **2007**, *45*, 1558−1565.
(30) Yang, S.; Zhi, L.; Tang, K.; Feng, X.; Maier, J.; Müllen, K. Efficient Synthesis of Heteroatom (N or S)-Doped Graphene Based on Ultrathin Graphene Oxide-Porous Silica Sheets for Oxygen Reduction Reactions. *Adv. Funct. Mater.* **2012**, *22*, 3634−3640.
(31) Xu, Y.; Bai, H.; Lu, G.; Li, C.; Shi, G. Flexible Graphene Films via the Filtration of Water-Soluble Noncovalent Functionalized Graphene Sheets. *J. Am. Chem. Soc.* **2008**, *130*, 5856−5857.
(32) Hummers, W. S., Jr; Offeman, R. E. Preparation of Graphitic Oxide. *J. Am. Chem. Soc.* **1958**, *80*, 1339.
(33) Zhao, Y.; Hu, C.; Hu, Y.; Cheng, H.; Shi, G.; Qu, L. A Versatile, Ultralight, Nitrogen-Doped Graphene Framework. *Angew. Chem., Int. Ed.* **2012**, *51*, 11371−11375.
(34) Wang, H.; Zhang, D.; Yan, T.; Wen, X.; Zhang, J.; Shi, L.; Zhong, Q. Three-Dimensional Macroporous Graphene Architectures As High Performance Electrodes for Capacitive Deionization. *J. Mater. Chem. A* **2013**, *1*, 11778−11789.
(35) Chen, C.-M.; Zhang, Q.; Huang, C.-H.; Zhao, X.-C.; Zhang, B.-S.; Kong, Q.-Q.; Wang, M.-Z.; Yang, Y.-G.; Cai, R.; Sheng Su, D. Macroporous "Bubble" Graphene Film via Template-Directed Ordered-Assembly for High Rate Supercapacitors. *Chem. Commun.* **2012**, *48*, 7149−7151.
(36) Choi, B. G.; Yang, M.; Hong, W. H.; Choi, J. W.; Huh, Y. S. 3D Macroporous Graphene Frameworks for Supercapacitors with High Energy and Power Densities. *ACS Nano* **2012**, *6*, 4020−4028.
(37) Zheng, Z.; Zheng, X.; Wang, H.; Du, Q. Macroporous Graphene Oxide−Polymer Composite Prepared through Pickering High Internal Phase Emulsions. *ACS Appl. Mater. Interfaces* **2013**, *5*, 7974−7982.
(38) Ding, W.; Wei, Z.; Chen, S.; Qi, X.; Yang, T.; Hu, J.; Wang, D.; Wan, L.-J.; Alvi, S. F.; Li, L. Space-Confinement-Induced Synthesis of Pyridinic- and Pyrrolic-Nitrogen-Doped Graphene for the Catalysis of Oxygen Reduction. *Angew. Chem., Int. Ed.* **2013**, *52*, 11755−11759.
(39) Yasuda, S.; Yu, L.; Kim, J.; Murakoshi, K. Selective Nitrogen Doping in Graphene for Oxygen Reduction Reactions. *Chem. Commun.* **2013**, *49*, 9627−9629.
(40) Lai, L.; Potts, J. R.; Zhan, D.; Wang, L.; Poh, C. K.; Tang, C.; Gong, H.; Shen, Z.; Lin, J.; Ruoff, R. S. Exploration of the Active Center Structure of Nitrogen-Doped Graphene-Based Catalysts for Oxygen Reduction Reaction. *Energy Environ. Sci.* **2012**, *5*, 7936−7942.
(41) Zhang, C.; Hao, R.; Liao, H.; Hou, Y. Synthesis of Amino-Functionalized Graphene As Metal-Free Catalyst and Exploration of the Roles of Various Nitrogen States in Oxygen Reduction Reaction. *Nano Energy* **2013**, *2*, 88−97.
(42) Li, N.; Hu, C.; Ren, L.; Cao, M. Temperature-Dependent Enhancement of Oxygen Reduction Reaction Activity for Interconnected Nitrogen-Doped Carbon Shells. *CrystEngComm* **2013**, *15*, 8504−8510.